

DEBLURRING ALGORITHM FOR VIDEO IMAGE BASED ON DENOISING ENGINE ALONG WITH CONTRAST ENHANCEMENT

Dr. S. Saravanan¹, S. Sai Sindhu², C. Dharani³, S. Pradeep Kumar⁴, T. Sai Krishna⁵

¹Associate Professor, Department of ECE, N.B.K.R Institute of Science and Technology, Vidyanagar, Tirupati, India.

^{2,3,4,5}B. Tech Student, Department of ECE, N.B.K.R Institute of Science and Technology, Vidyanagar, Tirupati, India.

I. ABSTRACT

To address the problem of blurred digital video losing inter-frame information and ignoring spatiotemporal during restoration, a video image deblurring approach based on a denoising engine is proposed. The term Laplacian regularization has been extended to the realm of video image restoration. First, we use the non-local means (NLM) regularization to extract redundant information from video image, and then we provide a novel restoration model that combines several regularizes, particularly the NLM regularize and the denoising regularize. To solve the video image restoration model, we use the simplest gradient descent approach. The experiment results show that our method has an excellent deblurring effect and is noise resistant along with enhancement.

Keywords—regularization by denoising, NLM, self-similarity video image deblurring.

II. INTRODUCTION TO MOTION DEBLURRING

With the advancement of camera technology, acquired image quality has greatly improved. However, there are always some flaws in photographing or hardware limitations that contribute to image degradation. With an open shutter, there is more chance of relative motion between an object and the

camera, which causes motion blur and is the most common type of degradation in the field of imaging. It ruins valuable information and introduces obnoxious artifacts into the observed image.

Motion blur can occur in three ways;

a) Blurred camera shake

Photographs are not captured instantly; rather, the acquisition process is spread out over time, which is known as exposure time. It is difficult to keep a handheld camera steady for an extended period of time while taking pictures.



Fig.1: Motion blur images due to camera shake

(a) Translation Blurred Image

(b) Images with rotational blur [1]

Camera shake can include translation and rotational phenomena. Blur caused by the camera's uniform velocity translation results in a global blurring effect known as Space invariant blur. Each image point is blurred equally, regardless of image pixel location. During convolution, the blurring function produces a uniform blurring effect for each pixel location.

The blurring effect is caused by camera rotation, which results in a Space variant blur. This is due to camera rotation; the blurring effect varies for different pixels and is dependent on the spatial position of the pixel in the image.

1) Motion blur of an object

Object motion blur occurs when a moving object in the scene, such as a moving car exhibit. Figure 2 shows motion blurred images due to object motion.



Fig.2: Motion Blurred images due to object motion [1]

1) Both the camera and the object are moving.

When cameras are mounted on a stand, there is the possibility of vibration, and the object in the scene is in relative motion with respect to the camera, causing the recorded image to blur. Figure 3 depicts motion blurred images caused by both the object and the camera moving.



Fig.3: Motion Blurred images due to combination of camera shake and object motion [1]

Correct information within the scene may be smeared out as a result of this motion blur effect, and some important observations may be missed. As a result, undoing such a blur effect and restoring the original information is a significant challenge. The reconstruction method used to recover the pristine image can be blind or non-blind depending on whether the degradation function is known or unknown. Blur effect in captured photograph and blind reconstruction method used when degradation function is unknown. Blind motion deblurring is a two-step problem that begins with determining the blurring function or point spread function (PSF) and ends with estimating the unblurred or original image. The block diagram for Blind motion deblurring / Blind image deconvolution is shown in Figure 4. (BID). Blind motion deblurring/ Blind image deconvolution (BID).

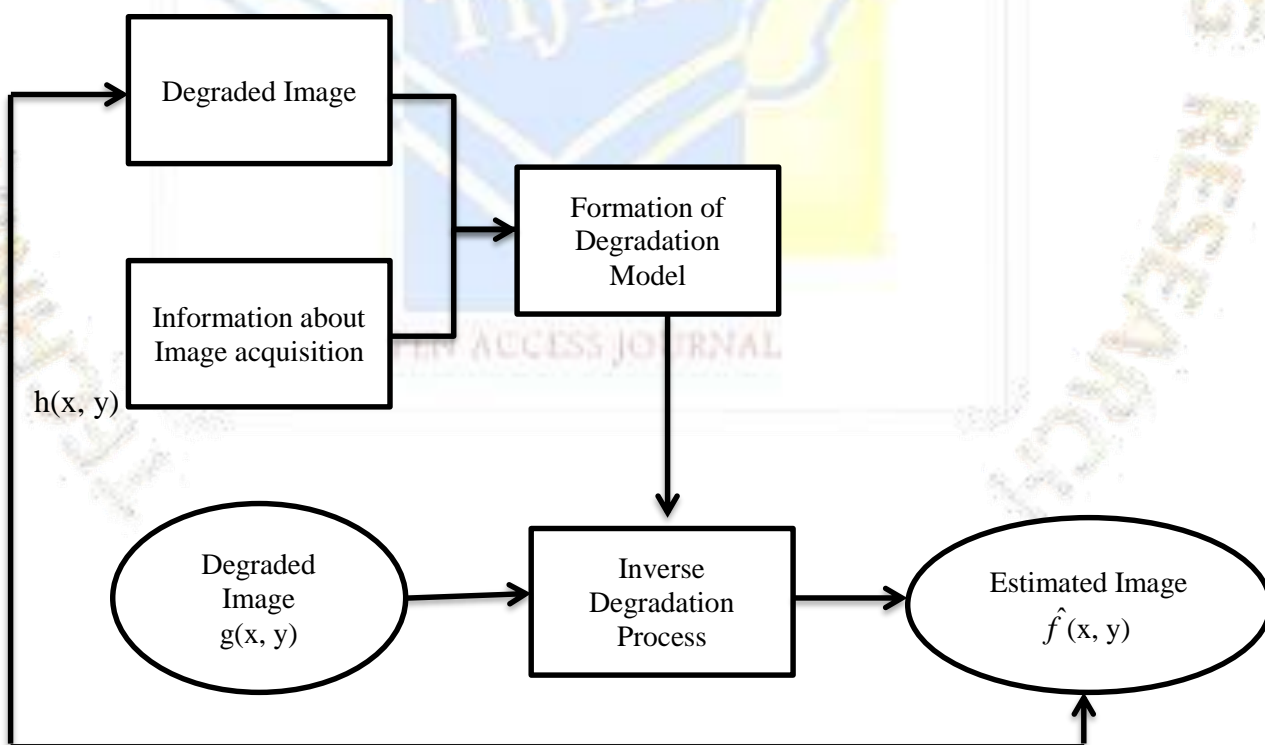


Fig.4. Block diagram of Blind motion deblurring

Challenges

- The goal of the BID problem is to produce a high-quality restored image by undoing the blurring effect. To remove the blurring effect, you must first understand the type and extent of image degradation. There has been a lot of research done to accurately estimate the degradation function (PSF) [89-116]. Any error in PSF estimation has a serious impact on restoration image quality, so accurate estimation of the degradation function is a critical issue in resolving the BID problem.
- The recorded scene is a convoluted PSF and sharp image with one output term represented by two unknown terms. The problem is ill-posed, with infinitely many solutions. It is difficult to find the correct solution without any prior knowledge of degradation or sharp image.
- Deblurring noise and ringing artifacts are generated during the deblurring process due to the restoration filter's inability to estimate the image data perfectly. Ringing artifacts are produced during the deblurring process as a result of incorrect PSF estimation, noise, or the inability of Fourier bases to model the image's edges. Figure 5 shows an example of a reconstructed image with ringing. Undoing these imperfections and reconstruct back the pristine image from single shot (single image) is a challenging task and considered as the main objective of this research.



(a)



(b)

Fig.5. Ringing effect observation in deblurred image (a) Blurred image (b) Reconstructed image with ringin

III.MOTIVATION OF RESEARCH WORK

In science and technology, recovering original output from a degraded version is a kind of universal inverse problem. This fundamental, but powerful reality drives us to create a method that can be used in a wide range of applications such as astronomical imaging, photo editing, medical imaging, and so on.

Researchers have been working on motion deblurring since the 1960s. The main difficulty stems from a lack of prior knowledge about the image or the blurring process, as well as a lack of optimal restoration filters to reduce or eliminate the blurring effect. Images/videos play an important role in our daily lives, and in many cases such as journalism, crime cases, family functions, outdoor scenes, amateur photography, or traffic surveillance if we wish, furthermore, blind deblurring is linked to other fields such as super resolution, painting, and denoising, among others. The use in a wide range of applications necessitates more simple, accurate, and efficient methods, necessitating ongoing research in the field of motion deblurring. It is an established discipline with a solid theoretical foundation and high-performance deconvolution algorithms for estimating the uncorrupted image. Advanced techniques for accurate PSF estimation and blind motion deblurring based on recent innovations are in high demand to solve a wide range of application problems in a simple and efficient manner. The identified area has potential for improving the efficiency of blind deblurring algorithms.

The main advantage of Hough transform techniques is that they are less affected by image noise and are tolerant of gaps in feature boundary descriptions. Lokhande [99] demonstrated that the Hough transform can be used to identify the anisotropic nature of blurred image spectrums observed perpendicular to the motion blur. The blur direction can be calculated from the log magnitude spectrum of the blurred image as the angle corresponding to the maximum value of the Hough transform minus 90 degrees. The blurred image's binarized spectrum is rotated anticlockwise by an estimated angle, and the 2-D spectrum is converted to 1-D spectrum. Blur length is measured as the first negative peak value of the inverse Fourier transform of a rotated binarized 1-D spectrum. If the blurring characteristic of the

image is indistinct, the effect of identifying direction of motion by this method would be unsatisfactory.

X. Y. Fang et al. [100] proposed a method that included pre-processing steps prior to the Hough transform. Han windowing is used to remove horizontal and vertical lines in the spectrum caused by boundary artifacts (leading to incorrect angle estimation). Many researchers have adopted this preprocessing step for blur identification tasks. Histogram equalisation is used to improve image contrast. Improved Hough transform-based method applied on Cepstrum of blurred image to increase blur angle estimation accuracy. They discovered a pixel set that was voted for blur direction estimation and used the least square line fitting method to re-estimate blur direction. Blur length is calculated by collapsing a 1-D spectrum.

Shiqian Wu et al. [101] proposed a method for detecting canny edges in binarized cepstrum using the Hough transform. They calculated the length by averaging and interpolating m cross section data from a logarithmic spectrum in a motion blurred image. Interpolation of a non-pixel point P and its intensity at point p are computed.

P. S. Prashanth Rao and Rajesh Kumar Muthu [102] investigated the use of the Hough transform on the Edge map of cepstrum for three colour channels, with the average of the measured angles from the three channels estimating the blur direction. To estimate the blur length accurately, the first negative peak of rotated collapsed 1-D cepstrum for three colour channels is observed, as well as the maximum value among them is considered as blur length. They demonstrated their performance in license plate deblurring.

Radon Transformation

M. E. Moghaddam and M. Jamzad [93] proposed using the radon transform to estimate blur direction. Steerable filters are less accurate, and the Hough transform requires a suitable candidate point to fit the line. In contrast, the Radon transform does not necessitate the specification of candidate points. They calculated the maximum value of the radon transform by applying it to the Log Fourier spectrum of a blurred image. The direction of motion blur is the corresponding angle minus 90 degrees. The valley distance computed from the 1-D power spectrum is used to estimate blur length.

If the image is not square, Felix Krahmer et al. [103] proposed modifying the radon transform. They proposed using the Radon transform to normalise the image by dividing the Radon transform values by the Radon transform of a matrix of 1's of the same dimension as the image. The Hanning window is suggested for smoothing the boundary problem. Before rotating the cepstrum, Gaussian filtering is applied, and a peak is observed. Peaks are seen at opposite angles to the origin and are amplified by reflected image addition. The blur length is the distance between the negative peak and the origin point. M. E. Moghaddam and M. Jamzad proposed a combined Radon transform and fuzzy set to calculate blur parameters in another method [104]. Extensive work with the radon transform and bispectrum modeling of white bounds has been observed [105] shows the power spectrum of a blurred image. They demonstrated that the lobe width (valleys position) in a 1D power spectrum corresponds to the mean of a bispectrum, and that function design curve fitting is used to determine the length of motion blur. A. M. Deshpande and S. Patnaik estimated blur angle and length using the Radon transform of a dual log -FFT operated blurred image [106].

IV.EXISTING WORK

Noise and blur are the most common image degradation problems in the field of short video and public security monitoring [1]. Several image restoration methods have been developed over the last few decades, primarily using regularization technology to add appropriate constraints to the original ill-conditioned problem and transform it into a benign problem in order to achieve image restoration. Such as TV regularization [2] and wavelet-based regularization [3]. It is worth noting that, unlike other image restoration problems, the performance of the image denoising algorithm approaches its limit. The ability to use an efficient denoising algorithm to deal with other image restoration issues becomes critical. [4], [5] propose a plug-and-play algorithm for decomposing the inverse problem of image restoration. Iterates through the successive application of image denoising into a series of image denoising tasks. Romano Y proposed in this context to build an adaptive Laplace regularization function using the denoising function [6], and to create a new regularization term by constraining the inner product of the input image and its denoising residuals. The proposed algorithm provides a strong model

framework for image restoration algorithms that are based on reconstruction. Different regularization terms can choose denoising function to construct regularization term based on the requirements of visual effect, time, and other performance indicators of image restoration. This paper extends the algorithm to the field of video image restoration, taking into account the flexibility and efficiency of the regularization term in the selection of the denoising function. The redundant information between and within video frames, and obtains a more rigorous video image restoration model by using NLM regularizations [7], [8] and denoising regularization to constrain the objective function. The experimental results show that the algorithm outperforms the PSNR index and the visual comparison.

V. EXISTING ALGORITHM

If we consider an image to be a vector of length n , the image denoising model is $y = x + e$, where x is the original image vector and y is the noise image vector. The noise vector has a normal distribution: $e \sim N(0, \delta^2 I)$. The denoising engine is a function $f: [0, 255]^n \rightarrow [0, 255]^n$, in order to construct regularization term by using denoising function, we mention that two conditions on $f(x)$ must be satisfied, I local homogeneity, that means $f(mx) = mf(x)$, $|m - 1|$ for a very small $\leq \epsilon$. Denote $\nabla_x f(x)$ as the directional derivative of $f(x)$ along x , which gives

$$\nabla_x f(x)x = \frac{f(x+\epsilon x) - f(x)}{\epsilon} \quad (1) \quad \text{Invoking}$$

local homogeneity we get

$$\nabla_x f(x)x = \frac{(1+\epsilon)f(x) - f(x)}{\epsilon} = f(x) \quad (2)$$

Another condition is (ii) strong passivity, which is defined as $\eta(\nabla_x f(x)) \leq 1$, where where $\eta(\nabla_x f(x))$ is the spectral radius of the Jacobian matrix $\nabla_x f(x)$. We have the following derivation here.

$$\|f(x)\| = \|\nabla_x f(x)x\| \leq \eta(\nabla_x f(x)) \cdot \|x\| \leq \|x\| \quad (3)$$

We get $f(x) = \nabla_x f(x)x$ and $\|f(x)\| \leq \|x\|$ when we satisfy local homogeneity and strong passivity. The high passivity ensures that the denoising function does not enlarge the norm of the original image. It has been discovered through research that a series of superior denoising algorithms, such as BM3D [9], trainable nonlinear reaction diffusion (TNRD) [10], all meet the above two situations, and these algorithms are composed of two stages: the first stage is to make a highly nonlinear decision, and the second stage is to use the decision to make

the linear filter adapt to the original noise image and perform the actual noise removal [11]. As an example, the denoising problem can be expressed as

$$X_{\text{Denoise}} = f(y) = W(y)y \quad (4)$$

where W is the $n \times n$ pseudo-linear filter matrix and y is the $n \times 1$ noise image vector. We can deduce from the previous formula that $W(y)$ is the Jacobian matrix $\nabla_y f(y)$. As an aside, another natural requirement for W is that it is row-stochastic, which implies that I this matrix is nonnegative and (ii) the vector 1 is an eigenvector of W . This implies that a denoiser $f(y)$ has no effect on a constant image. Consider the description of the denoiser in (4), which motivates us to construct the Laplacian form as follows:

$$\begin{aligned} \rho_L(x) &= \frac{1}{2} x^T L(x)x = \frac{1}{2} x^T (I - W(x))x \\ &= \frac{1}{2} x^T (x - W(x)x) \end{aligned} \quad (5)$$

As a result, we get the more general definition of the Laplacian regularizer as follows.

$$\rho_L(x) = \frac{1}{2} x^T (x - f(x)) \quad (6)$$

Natural images contain a lot of redundant information. Using non-local self-similar prior knowledge of images, the classic NLM algorithm is obtained. To begin, the image is divided into several image blocks, and the similar neighbor blocks of the image block containing the target pixel are searched in a large window. The weighting factor of each similar neighborhood is then calculated, and the estimated value of the target pixel can be obtained by taking the weighted average of the image block's central pixel with the highest similarity. However, there is a lot of redundant information between adjacent frames in the video image. Figure 6 depicts the self-similarity of video images.

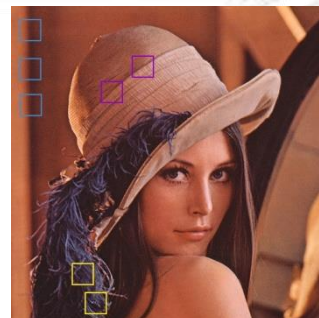


Fig.6. Example of self-similarity of video image. The squares marked with the same color are on similar images areas.

The adjacent frames before and after the target frame are used as reference frames in this paper, and the number of reference frames is denoted by L. Extending the search range for related image blocks. The following equation can be used to solve the weighting factor s_{ij} .

$$s_{ij} = \exp\left(\frac{-\|N_i - N_j\|_2^2}{h^2}\right) \quad (7)$$

N_i is the image block with the center pixel I and I is the current pixel position. N_j is the neighbor block with the center pixel j, and c is the weighting attenuation smoothing parameter. After obtaining the weighting factor of pixels in the search window, sort in descending order and estimate the first q weight set $C(x_i)$. Convert the set of weights for each pixel into a row vector to obtain the weight matrix for the entire image.

$$S_{i,j} = \begin{cases} s_{i,j}, & j \in C(x_i) \\ 0, & \text{else} \end{cases} \quad (8)$$

Therefore, the NLM regular term can be written as follow:

$$\rho_{NLM}(x) = \sum_{i=1}^n \|x_i - Sx\|_2^2 = \|(I - S)x\|_2^2 \quad (9)$$

where I is the $n \times n$ identity matrix. S is the weight matrix of the proposed algorithm, and x is the column vector of the input image. The blurred image restoration model can be expressed as $y = Hx + e$, where H is the blurred operator and e is WGN contamination of variance 2δ . In this case, the MAP problem becomes.

$$x = \underset{x}{\operatorname{argmin}} \frac{1}{2\delta^2} \|Hx - y\|_2^2 + \lambda \rho(x) \quad (10)$$

Construct a new model by combining the above-mentioned denoising regular term and the NLM regular to constrain the objective function:

$$x = \underset{x}{\operatorname{argmin}} \frac{1}{2\delta^2} \|Hx - y\|_2^2 + \frac{\lambda}{2} x^T (x - f(x)) + \theta \|(I - S)x\|_2^2 \quad (11)$$

Denote, then the overall energy functional to minimize is:

$$E(x, y) = l(x, y) + \frac{\lambda}{2} x^T (x - f(x)) + \theta \|(I - S)x\|_2^2 \quad (12)$$

The gradient of this expression is readily available by

$$\begin{aligned} \nabla_x \rho_L(x) &= \frac{\lambda}{2} \nabla_x \{x^T (x - f(x))\} \quad (13) \\ &= \lambda x - \frac{\lambda}{2} (f(x) + \nabla_x f(x)x) \\ &= \lambda(x - f(x)) \end{aligned}$$

$$\nabla_x E(x) = \nabla_x l(y, x) + \lambda(x - f(x)) + 2\theta(I - S)^2(I - S)x \quad (14)$$

To solve the model, the simplest gradient descent method algorithm can be used, which is updated as follows.

$$x_{k+1} = x_k - \mu \{ \nabla_x l(y, x)|_{\hat{x}_k} + \lambda(x_k - f(x_k)) + 2\theta(I - S)^T(I - S)x_k \} \quad (15)$$

Overall, the proposed algorithm is summarized as follows:

Input: Target frame X and adjacent reference frame

Regularization parameter λ and θ .

Denoising algorithm f .

Number of iterations N

$K = 1$

Initialization: set $x_0 = y$

While not converged and $k \leq N$ do update

the solution by

$$x_{k+1} = x_k - \mu \left\{ \frac{1}{\delta^2} H^T (Hx_{k-1} - y) + \lambda(x_k - f(x_k)) + 2\theta(I - S)^T(I - S)x_k \right\}$$

End while

Result the above algorithm produces the X_N .

The experiments are divided into two sections in this section. In the first part, we examine the restoration of a video image using two different blur kernels. In the second part, run deblurring experiments on video images with various reference frames. A Comparison of Different Video Image Deblurring Algorithms The video images needed for the experiment are from the standard video test library and are all 352×288 pixels in size (CIF format). The experiment employs two types of blur kernels: a 9×9 uniform blur and a 5×5 Gaussian blur with a standard deviation of 1.6. A Gaussian white noise with a standard deviation of 2 is added in both cases the blurred image. The TNRD algorithm is the denoising engine that we use. We chose to use the suggested gradient descent method for $N = 400$ iterations with $\lambda = 0.12$ for uniform blur and $N = 200$ iterations with $\lambda = 0.22$ for Gaussian blur. $\theta = 0.15$ and $L = 2$ are the NLM regularization parameters. In terms of image deblurring, the TV algorithm, the nonlocally centralized sparse representation (NCSR) algorithm, and the Regularization by Denoising (RED) algorithm are used to compare

with the proposed method.

As seen, this algorithm has a positive effect on image details and edges, bringing the restored video image closer to the original video image B. Restoration Outcomes in Various Reference Frames The first part of the experiment is run with $L=2$, and now we consider changing the number of reference frames. When $L = 0$, the inter-frame redundancy prior of the video is not taken into account. When $L = 2$, choose one frame before and one frame after the target frame. Likewise, $L = 4$ and $L = 6$. The restoration results of the seventh frame of the video Waterfall and Foreman under Gaussian blur are shown in Fig. 7.

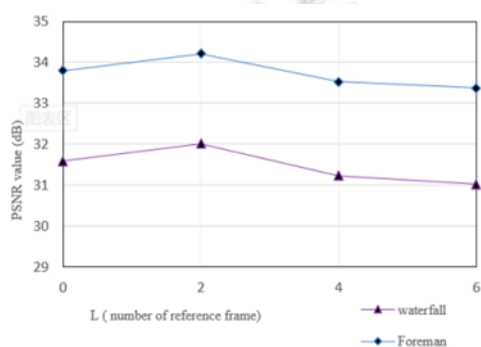


Fig.7: Comparison of the PSNR value versus the number of reference frame for video image

The line graph shows that the PSNR value of the two video images is lower when $L = 0$. The PSNR value reaches its maximum when the number of reference frames is increased to $L = 2$. At this point, increasing the number of reference frames reduces the PSNR value. This demonstrates that increasing L causes too much noise, which affects the model's restoration.

VI. PROPOSED WORK

Video Resolution Enhancement

The FT is a commonly used tool in the transform domain for signal processing and analysis. However, the FT is ineffective for non-stationary signal analysis. To address this issue, the DWT is used for non-stationary signal analysis. The use of DWT is limited due to certain drawbacks such as large memory requirements due to the use of filters, limited perfect reconstruction, and computationally complex structure. Because of its appealing features such as low-rank approximation, lower computational complexity, and so on, SVD has become a popular algebraic transform in a variety of image processing applications in recent years. When dealing with non-stationary signals, adaptive transforms are preferable to fixed transforms. One possible solution to these problems is the MR-SVD. The

MR-SVD is a data-dependent adaptive algorithm. There is no fixed set of basis vectors in the adaptive transform. It is both perfect for reconstruction and simple. In recent years, MR-SVD has been used in a variety of image processing applications such as image compression, denoising, and fusion. The application of MR-SVD for image CE is discussed in this chapter.

Histogram equalization of a colour image in RGB colour space is accomplished by extracting R, G, and B component images from the colour image and then equalizing the resulting histograms separately for R, G, and B component images. Histogram equalization of colour image components on their own can usually result in erroneous colour. Another approach is to uniformly equalize the colour intensities without changing the colours. The RGB colour space image is first converted to HSI colour space. Only the intensity component is equalized; the hue and saturation components remain unchanged. The image in HSI colour space is converted back to RGB colour space after equalization. In the histogram plots, three curves in three different colours (Red, Green, and Blue) are shown represents the intensity level variation in three colour planes (red, green, and blue). The image enhanced in HSI colour space retains the natural colors shown. Even though intensity equalization has no effect on the image's hue and saturation values, it does have an effect on overall colour perception. The saturation component can be adjusted to correct this.

The proposed DWT-SVD-based CE technique for grey scale images is extended to colour images in RGB and HSI colour spaces by following the general approach specified for enhancing colour images using grey scale techniques. The first step is to determine whether the given image is gray scale or color. If the image is in colour, the following method is used. The following is a step-by-step procedure for implementing the proposed DWT-SVD-based image CE technique in HSI colour space:

Step 1: The low contrast RGB colour image input is converted to HSI colour space.

Step 2: In the following steps, I divided the HSI colour image into three sub-images (H, S, and I) and processed only the intensity sub-image.

Step 3: The GHE is applied to the input image's intensity sub-image.

Step 4: To obtain four sub-band images, the DWT is applied to the intensity sub-image of the image obtained in Step 2 and the histogram

equalized intensity sub-image obtained in Step 3. (LL, LH, HL, and HH).

Step 5: Singular value matrices for LL sub-band images of input and histogram equalized intensity sub-images obtained in Step 4 using SVD.

Step 6: Maximum singular values are calculated using the input and histogram equalized intensity sub-image singular value matrices obtained in Step 5.

Step 7: The correction factor is determined.

Step 8: For the intensity sub-image, the modified singular value matrix and modified LL sub-band image are obtained.

Step 9: To obtain a contrast-enhanced intensity sub-image, IDWT was applied to the modified LL sub-band image obtained in Step 8 as well as the LH, HL, and HH sub-band images of the input image obtained in Step 4.

Step 10: The contrast-enhanced intensity sub-image obtained in Step 9 is concatenated with the hue and saturation images obtained in Step 2 to produce the contrast-enhanced output colour image in HSI colour space.

Step 11: The HSI colour space enhanced image is converted to RGB colour space.

The following is a step-by-step procedure for implementing the proposed DWT-SVD-based image CE technique in RGB colour space:

Step 1: A low contrast RGB image is divided into three sub-images given as input (R, G, and B).

Step 2: The GHE is used on three sub-images of the original image.

Step 3: The DWT is applied to the three sub-images obtained in Steps 1 and 2 to produce four sub-band images (LL, LH, HL, and HH) of the original input image and the histogram equalized image.

Step 4: For three sub-images of input and histogram equalized images obtained in Step 3, the SVD is used to obtain singular value matrices of LL sub-band images.

Step 5: The singular value matrices of all sub-images of the input and histogram equalized image obtained in Step 4 are used to calculate the maximum singular values.

Step 6: Three sub images are used to compute the correction factors.

Step 7: For three sub-images, modified singular

value matrices and modified LL sub-band images are obtained.

Step 8: The IDWT is applied to the obtained modified LL sub-band image.

Step 9: To obtain contrast-enhanced images for three sub-images, obtain LH, HL, and HH sub-band images of the input image obtained in Step 3.

VII.RESULTS

Run your code and paste the results here

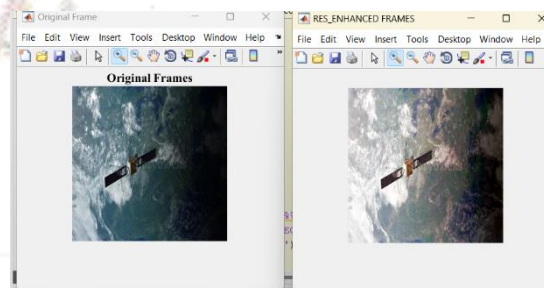


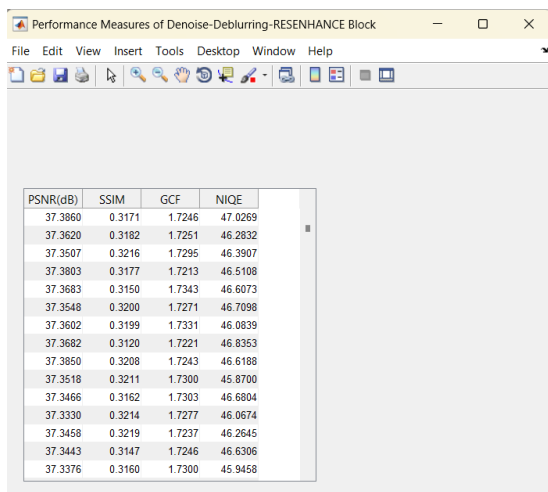
Fig 8: Comparison of original frames and noise, blur free enhanced frames.

PSNR(dB)	SSIM	GCF	NIQE
30.4821	0.5401	1.7352	4.4837
30.4938	0.5402	1.7389	4.2865
30.4900	0.5393	1.7403	4.2874
30.5004	0.5377	1.7311	4.4522
30.4810	0.5344	1.7414	4.3939
30.5426	0.5341	1.7460	4.4186
30.5422	0.5379	1.7514	4.2886
30.5212	0.5350	1.7388	4.3791
30.5691	0.5382	1.7426	4.4954
30.5782	0.5347	1.7201	4.3120
30.5591	0.5381	1.7391	4.4554
30.5460	0.5346	1.7283	4.4127
30.5215	0.5347	1.7443	4.3370
30.5705	0.5318	1.7395	4.4827
30.6025	0.5336	1.7384	4.3642

Table.1: Performance Measure of Denoising Block

PSNR(dB)	SSIM	GCF	NIQE
30.5119	0.5286	1.9135	2.4894
30.5272	0.5314	1.9131	2.6038
30.5166	0.5295	1.9173	2.6145
30.5417	0.5280	1.9140	2.5029
30.5412	0.5239	1.9171	2.5334
30.5414	0.5317	1.9158	2.5716
30.5731	0.5277	1.9179	2.6442
30.5818	0.5227	1.9144	2.5621
30.5997	0.5261	1.9134	2.4816
30.6094	0.5317	1.9159	2.6808
30.6145	0.5267	1.9156	2.5349
30.6079	0.5278	1.9144	2.6123
30.5806	0.5257	1.9130	2.6118
30.6135	0.5260	1.9130	2.5402
30.6267	0.5259	1.9173	2.6033

Table.2: Performance Measure of Denoising-Deblurring Block



PSNR(dB)	SSIM	GCF	NIQE
37.3860	0.3171	1.7246	47.0269
37.3620	0.3182	1.7251	46.2832
37.3507	0.3216	1.7295	46.3907
37.3803	0.3177	1.7213	46.5108
37.3683	0.3150	1.7343	46.6073
37.3548	0.3200	1.7271	46.7098
37.3602	0.3199	1.7331	46.0839
37.3682	0.3120	1.7221	46.8353
37.3850	0.3208	1.7243	46.6188
37.3518	0.3211	1.7300	45.8700
37.3466	0.3162	1.7303	46.6804
37.3330	0.3214	1.7277	46.0674
37.3458	0.3219	1.7237	46.2645
37.3443	0.3147	1.7245	46.6306
37.3376	0.3160	1.7300	45.9458

Table.3: Performance Measure of Denoising-Deblurring-Enhancement.

VIII.CONCLUSION

In this project, we created NLM regularization terms for the regularization framework by searching for self-similar blocks between video frames. The video restoration model is then constrained using NLM regularization and denoising regularization. Experiments that optimized and enhanced the deblurring algorithm for video images validated the algorithm's logic. It has a specific application value for video restoration with significant scene changes.

IX.REFERENCES:

- [1] S. Farsiu, M. D. Robinson, M. Elad and P. Milanfar, "Fast and robust multiframe super resolution," in IEEE Transactions on Image Processing, vol. 13, no. 10, pp. 1327-1344.
- [2] A. Marquina and J. S. Osher, "Image Super-resolution by Tvregularization and Bregman Iteration," in J Sci Comput, Vol.37, no.3, pp.367-382
- [3] D. Cho, T. D. Bui, and G. Y. Chen., "Multiwavelet statistical modeling for image denoising using wavelet transforms" in Signal Process. Image Communication, vol. 20, pp. 77-89
- [4] S. V. Venkatakrisnan, C. A. Bouman and B. Wohlberg, "Plug-and-Play priors for model based reconstruction," 2013 IEEE Global Conference on Signal and Information Processing, Austin, TX, USA, 2013, pp. 945-948
- [5] A. Brifman, Y. Romano and M. Elad, "Turning a denoiser into a superresolver using plug and play priors," 2016 IEEE International Conference on Image Processing (ICIP), Phoenix, AZ, USA, 2016, pp. 1404-1408

[6] Y. Romano, M. Elad, and P. Milanfar, "The Little Engine that Could: Regularization by Denoising," in SIAM Journal on Imaging Sciences, vol. 10, pp. 1804-1844

[7] M. Protter, M. Elad, H. Takeda and P. Milanfar, "Generalizing the Nonlocal-Means to Super-Resolution Reconstruction," in IEEE Transactions on Image Processing, vol. 18, no. 1, pp. 36-51, Jan. 2009

[8] W. Dong, L. Zhang, G. Shi and X. Li, "Nonlocally Centralized Sparse Representation for Image Restoration," in IEEE Transactions on Image Processing, vol. 22, no. 4, pp. 1620-1630, April 2013

[9] H. C. Burger, C. J. Schuler and S. Harmeling, "Image denoising: Can plain neural networks compete with BM3D?," 2012 IEEE Conference on Computer Vision and Pattern Recognition, Providence, RI, USA, 2012, pp. 2392-2399

[10] Y. Chen and T. Pock, "Trainable Nonlinear Reaction Diffusion: A Flexible Framework for Fast and Effective Image Restoration," in IEEE Transactions on Pattern Analysis and Machine Intelligence, vol. 39, no. 6, pp. 1256-1272, 1 June 2017

[11] Y. Dar, A. M. Bruckstein, M. Elad and R. Giryes, "Postprocessing of Compressed Images via Sequential Denoising," in IEEE Transactions on Image Processing, vol. 25, no. 7, pp. 3044-3058, July 2016